Experiments and Modeling of Large-scale Benchmark Enclosure Fire Suppression

SAM S. YOON*

Mechanical Engineering, Korea University, Anam-dong 5-Ga, Sungbuk-gu, Seoul, 136-713, Korea

VICTOR FIGUEROA, ALEXANDER L. BROWN AND THOMAS K. BLANCHAT

Fire & Aerosol Science Department, Sandia National Laboratories PO Box 5800 MS1135, Albuquerque, NM 87185 USA

(Received March 16, 2008)

ABSTRACT: This article presents a series of experiments on benchmark fire suppression. The experiments were performed in a controlled environment, utilizing a cylindrical object or calorimeter centered above a 2 m diameter pan filled with kerosene-based hydrocarbon fuel, JP8. The experimental setup and procedure for gathering data on water suppression performance are presented. The characteristics of the nozzles used in the experiments are presented as well. The experimental results provide the boundary condition and temporal data necessary for validation of the fire suppression models used. The article also includes simulation results on the fire suppression experimental tests. The suppression simulations were carried out using a numerical model based on a Temporally Filtered Navier-Stokes (TFNS) formulation coupled with a Lagrangian model for droplets, which includes detailed descriptions of the interaction between the water droplets and the fire plume. The results from both experiments and simulations suggest that the criterion for complete suppression depends on a combination of factors including the mass flow rate (or nozzle diameter), nozzle operating pressure, and calorimeter presence. A critical regime which distinguished the regions of suppression and no-suppression in the domain of the mass flow rate versus operating pressure is found.

*Author to whom correspondence should be addressed. E-mail: skyoon@korea.ac.kr
Figures 1–18 appear in color online: http://jfs.sagepub.com

0734-9041/10/02 0109–31 $10.00/0 DOI: 10.1177/0734904109104503
© SAGE Publications 2010
Los Angeles, London, New Delhi and Singapore

KEY WORDS: fire suppression model, water mist, compartment fire.

INTRODUCTION

FIRE FIGHTING HAS great impact on the rescue of human lives and on the thermal damage of man-made structures. To alleviate the danger posed by unexpected fires, water sprays have been used as a common fire suppression tool mainly because of their low-cost operation, nontoxicity, and highly effective suppression capability. The fairly high latent heat of vaporization for water enables the absorption of a large amount of heat from fires. The interest in utilizing water as a suppressant has substantially grown since the Montreal Protocol in 1987, which required the banning of ozone-depleting halon as a suppressant [1]. While the use of water has received much attention as an alternative fire-fighting agent, the optimization of water spray systems has been an on-going issue, which has deserved extensive research [2,3].

For example, a limited amount of suppressant should be presumed in the optimization of a suppression system. If the suppressant is insufficient the suppressant might be depleted before the suppression of the targeted thermal hazard. For this reason, the trend or behavior of fire suppression under a given suppressant mass restriction needs to be understood with reasonable depth or prediction for a given sizable fire. This research focuses on transportation related accidents involving fuel spill and ignition, which necessitate active suppression systems. For such accident scenarios, a high-momentum spray or water mist system is useful for quickly dispersing condensed suppressants onto the fire and the surrounding compartment to minimize the thermal hazard to its occupants.

Early pool fire suppression work can be found in Rasbash and Rogowski [4]. Their kerosene pool fire (30 cm in diameter) was cooled by downward projecting water sprays. They found that a spray system that produced smaller droplets resulted in more efficient extinguishment of fire. Novozhilov et al. [5] numerically simulated the burning and extinguishment of solid PMMA (polymethylmethacrylate) via a water spray. Simulation of methanol pool fire was provided by Prasad et al. [6]. Ndubizu et al. [7] experimentally showed the difference of the burning rate and extinguishment characteristics between heptane and JP8. Because the boiling temperature of JP8 was higher than that of heptane, water droplets were subject to greater heat when in contact with the fuel surface, resulting in quicker suppression. Heptane pool fires and their suppression were studied by Back et al. [8] and Back and Hansen [9],

and a quasi-steady-state model was also developed and validated against their own experimental data. Heskestad [10] provided a correlation for an optimized nozzle diameter in terms of water-spray mass flow rate and discharging water momentum. The correlation showed reasonably good agreement with the experiment conducted using a methane gas plume of 0.1–0.3 m in diameter. More recently, Adiga et al. [11] simulated the suppression of a pool-like gas-fire, without solving the formulations of the chemical reaction and radiation of the fire, by simulating an ultra fine water mist as the total flooding agent. More detailed literature reviews on the studies of pool fires and their suppression are available in ref. [3]. Most of the above-described tests are small scale, and laminar. Around 1 m diameter, pool fires transition to turbulent fires, and therefore behave differently.

While most of the aforementioned studies are circumscribed by standard bench scale tests (i.e., cup-burner size), our uniquely large-scale turbulent experiments and their fully 3D simulations offer an advancement of this field of study. A series of new fire benchmark tests were conducted to predict thermal hazards and their subsequent suppressions. The fuel used was hydrocarbon JP8 because the fuel spill scenario in air transportation applications is the focus of our study. Although the indoor fire test facility at Sandia National Lab (SNL) permits testing of a pool fire of sizes up to 3 m in diameter, a 2 m JP8 pool fire is examined in these tests. The tests are designed to identify whether or not suppression would be achieved for a given operating pressure and mass flow rate of the water suppressant. Test description and results are followed by an exercise illustrating the current modeling capabilities. This exercise helps validate our current existing model for the large-scale fire suppression scenarios.

EXPERIMENT SETUP AND PROCEDURE

The FLAME/Radiant Heat (FRH) test cell is part of the new Thermal Test Complex at Sandia National Laboratories. Figure 1 shows the FRH test cell with a pool fire at the ground level, the pipes that supply air flow to the test cell, the combustion by-products outlet chimney, and the instrumentation rooms outside the test cell. The test cell is cylindrical (18.3 m inner diameter) and has a height of 12.2 m. The ceiling slopes 18° upwards from the perimeter walls to a height of 14.6 m over the center of the facility. A round hole at the top of the facility (4.9 m diameter) transitions to a 3.0 m by 3.7 m chimney duct. The outer walls are made of steel channel sections and are filled with water to maintain a relatively

constant wall temperature during tests. The ground level of the FRH can be divided into three concentric sections: (1) the liquid fuel (JP8, methanol, etc.) pan or gas (H_2, methane, He, etc.) burner (maximum size is 3 m in diameter), (2) the spill plates, and (3) the grating for inlet combustion air. Air enters the FRH cell through a 3.05 m diameter pipe and is distributed via 18 supply pipes to an annulus located along the sub-basement circumference. Air entering the cell ground level was characterized experimentally and was shown to be uniform within 10% of the mean flow [12].

Figure 2 shows a test apparatus simulating a single-nozzle, water suppression system assembled inside FLAME. A 2 m long calorimeter was used to simulate the effects of fire suppression on engulfed objects. The steel calorimeter was 0.3 m in diameter and was located ~0.7 m above the top of the pan. All tests were conducted using a 2 m diameter fuel pan. A diesel-powered high pressure, high-volume spray pump fed various nozzles via a nominal 1.5 diameter plumbing.

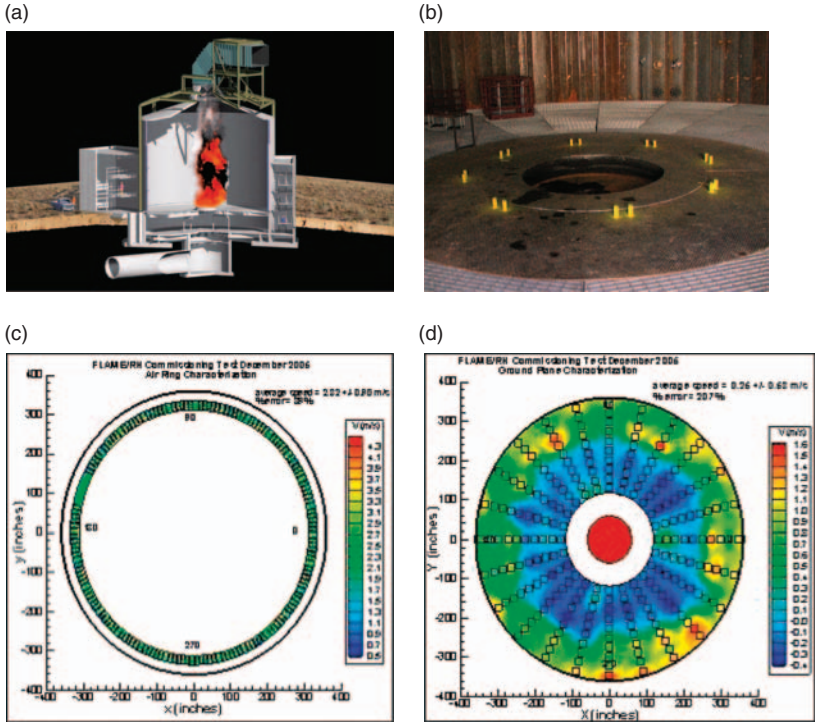

Figure 1. (a) FLAME test cell, (b) 2 m diameter liquid fuel pan, (c) Velocities at the air ring in the basement, (d) and at the ground level.

Two spray-angle configurations (45 and 90°) were tested. In the 90° configuration, the nozzle was positioned directly above the center of the pan. In the 45° configuration the nozzle was slightly <4.0 m from the center of the pan. In both configurations, the nozzle was ~ 5 m from the top of the pan.

All nozzles (Table 1) used in these experiments were 30°, full-solid-cone type supplied by *Spraying Systems*, Co., Wheaton, IL. As opposed to a nozzle of the hollow cone type, the full-solid-cone nozzle gives a uniform, round, fully dense spray with droplets of medium-to-large size. Pressure vs. mass flow rate characteristic curves were obtained for all nozzles. In addition, droplet information was obtained for all, but two nozzles: 3014 (0.094 in.) and 3050 (0.172 in.). A Phase Doppler Particle Analyzer was applied to obtain droplet volume, diameter, and droplet velocity 1 m from the exit of the nozzle axially, and at three different radial locations along the diameter of the nozzle spray, starting from the center; i.e., 0.0, 0.1, and 0.2 m.

Figures 3 shows flow rate-pressure data (with curve fits) for all four nozzles in addition to the droplet volume mean diameters and velocities

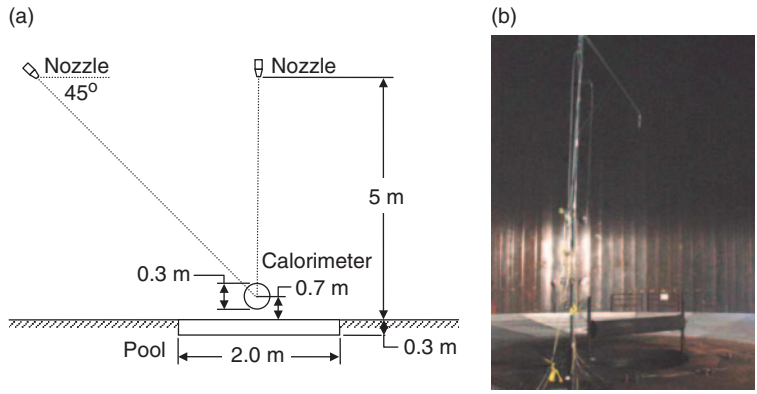

Figure 2. Experiment setup and nozzle configurations.

Table 1. Nozzle data.

Nozzle model no.	Nozzle diameter (in.)
30200	0.344
30400	0.469
3014	0.094
3050	0.172

for the two characterized nozzles. The volume mean diameter (VMD), $D_{0.5}$, expresses the droplet size in terms of the volume of the liquid sprayed. The VMD represents a value where 50% of the total volume (or mass) of the liquid sprayed is made up of droplets with diameters larger than the mean value and 50% smaller than the mean value. Note that the mean diameter decreases as the injection velocity increases. Since the Weber number increases as the velocity increases, the droplet size is naturally reduced in response to the balance between momentum induced drag force and surface tension.

Water line pressure was monitored upstream of the nozzle in each test. Four video cameras, enclosed by a water-cooled protecting shield, were placed at four different locations inside of FLAME. Two cameras recorded normal and parallel views of the fire; a third camera recorded the fire from above; and the fourth camera monitored for spillage below the floor plane. Before each test, JP8 was poured on top of a water layer sitting on the 2-m diameter pan, nominally providing a 3-min duration fire. Although fuel burn rates for this test were not actively measured, other nearly identical tests (for a different test series, same fire configuration) suggested a burn rate of 0.038 kg/(m^{2}s) with a standard deviation of 0.0016 kg/(m^{2}s). These burn rates were comparable with others found in the common literature within a factor of about 2 [13–15]. The total heat release rate was ~5 MW. A forced draft fan maintained an air flow rate of 150,000 ft^3/min. After about 1–2 min the fire was fully

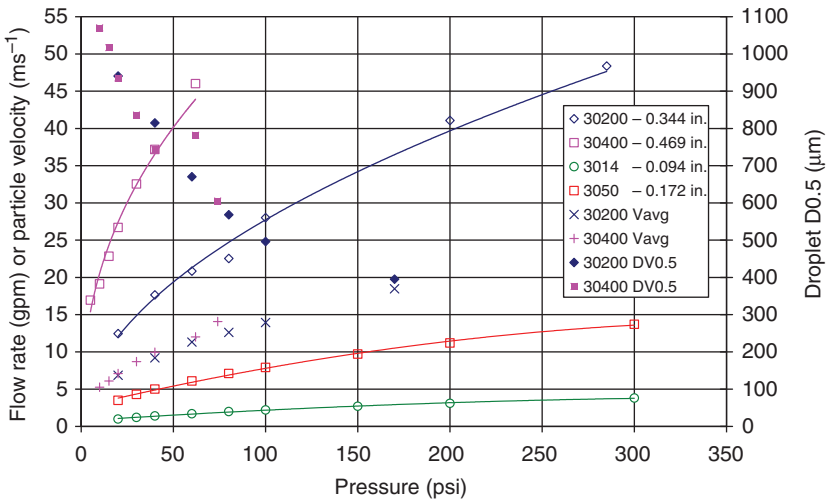

Figure 3. Nozzle flow rate and droplet mean diameter and velocity as a function of pressure, measured along the spray centerline at a distance of 1 m from the nozzle.

developed and the suppression system was activated. Suppression flows were active for about 30–40 s or until real-time video evidence suggested the fire was extinguished, whichever was shortest.

EXPERIMENTAL RESULTS

A total of 12 fire suppression benchmark test cases, comprising of 8 and 4 separate tests for 90 and 45° nozzle configurations, respectively, were conducted in the new FLAME facility. The following parameters were varied in these tests: (1) the position of the spray injection at injection angles of 45 and 90°, (2) operating pressures, (3) and the existence of the calorimeter directly above the pool fire.

Tables 2 and 3 show test runs for 90 and 45° nozzle angles, respectively. Two test runs were performed for each test, one *with* and one *without* a calorimeter. In addition, each test run was repeated twice to test the repeatability of results, so a total of 48 experimental runs were performed. Results showed that while the 90° test cases were repeatable, the 45° test cases were not in all cases.

Table 2. Test cases for 90° angle experiments.

Test no.	Operation pressure (psi)	Flow rate (gpm)	Nozzle model no./diameter (in.)
1	52	42	30400/0.469
2	74	48	30400/0.469
3	190	39	30200/0.344
4	25	14	30200/0.344
5	100	28	30200/0.344
6	155	34	30200/0.344
7	317	4	3050/0.094
8	317	14	3014/0.172

Table 3. Test cases for 45° angle experiments.

Test no.	Operation pressure (psi)	Flow rate (gpm)	Nozzle model no./diameter (in.)
1	25	14	30200/0.344
2	100	27	30200/0.344
3	155	34	30200/0.344
4	190	39	30200/0.344

Injection Angle of 90°

Figure 4 summarizes results of suppression tests with the 90° nozzle configuration. The arrows in the figure point to the operating conditions of the test run. The labels 'Supp' and 'No Supp' in the figure indicate the regime where suppression was or was not achieved, *without* the calorimeter. It is supposed that suppression was achieved when the flame was no longer observable in the video recordings.

As Figure 4 shows, for a single nozzle, suppression was achieved when the operating flow rates and pressures were on the high end of the nozzle operating curve. For example, in the case of nozzle 30200 (0.344 in. nozzle diameter), suppression was not achieved *with* and *without* the calorimeter when the flow rate was 14 gpm (Test 4). For the same nozzle, suppression was achieved *without* the calorimeter when the flow rate was 28 gpm (Test 5). Finally, for the same nozzle, suppression was achieved *with* and *without* the calorimeter at greater flow rates (Test 6 and Test 3), indicating the fact that high mass flow rate guarantees suppression regardless of the presence/absence of the calorimeter.

Similar trends were observed with nozzle 30400 (0.469 in. nozzle diameter), although at different operating conditions and in only two tests. In the case of nozzle 3050 (0.172 in nozzle diameter), suppression

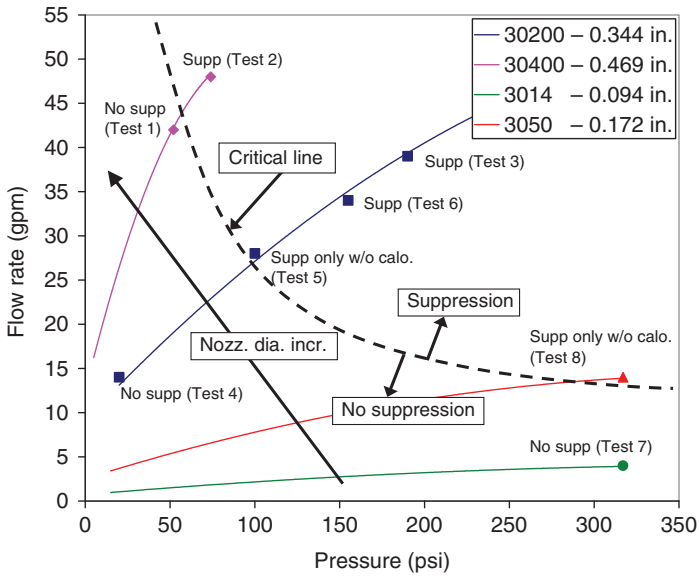

Figure 4. Summary results of the suppression tests.

was achieved *without* the calorimeter at 14 gpm, the highest flow rate the suppression system could operate with this nozzle. For nozzle 3014 (0.094 in nozzle diameter), suppression was not achieved *with* and *without* the calorimeter. Due to the limitations of the suppression system, the highest possible flow with nozzle 3014 was 4 gpm.

Figure 5 shows the time series snapshot of the fire suppression conducted with nozzle 30200 at 28 gpm flow rate *without* the calorimeter. The image taken at $t = -0.33$ s shows a typical fire prior to the spray injection. The time at which the water spray was first injected was regarded as the zero-time, $t = 0.00$ s. Figure 5 shows that the fire was suppressed when the calorimeter was not present. Here, the suppression time is defined as the time at which the fire is not *visible* in the images. In reality, the fire was extinguished near the fuel surface at a slightly earlier time, even though flames remained visible in the upper region of the fire. Notice that when the spray reached the flame – shown in the snapshots from $t = 0.33$ to 1.67 s – the extent of the fire appears to

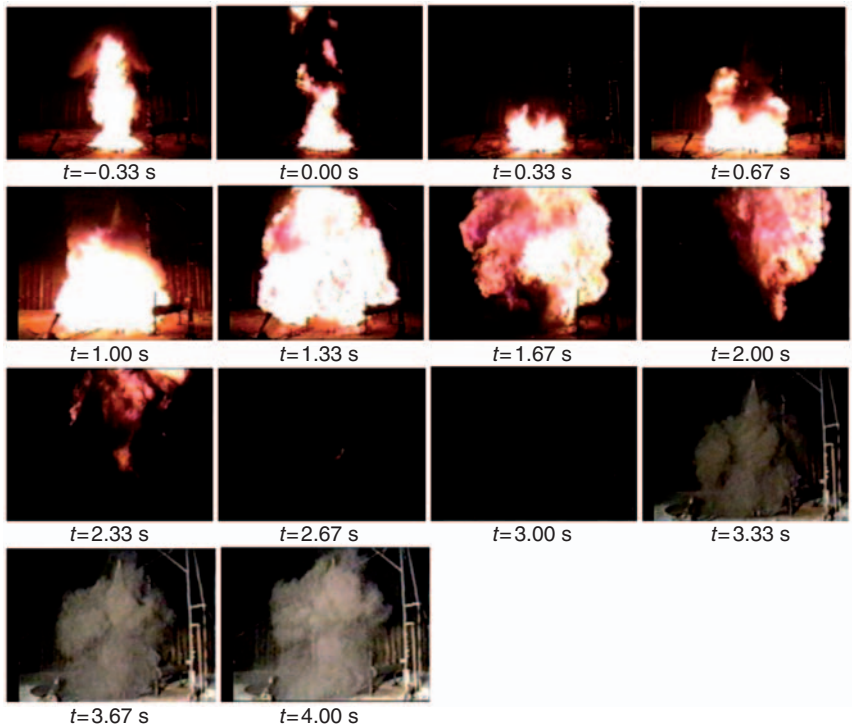

Figure 5. 90° spray injection at 100 psi without the calorimeter (Test 5). (Suppression is achieved at approximately $t = 3 \pm 0.33$ s).

increase, presumably resulting in an increase in heat flux in the vicinity of the fire. The increase in fire intensity is caused by an enhanced fuel-mixing rate. In this case, the spray momentum was sufficiently high to reach the fuel surface; therefore, suppression was achieved. A rough estimate of the momentum of an individual droplet is, $\rho_{H_2O}(\pi/6)D_{0.5}^3 V_{1m}$, where $D_{0.5}$ is the measured droplet diameter and $V_{1\mathrm{m}}$ is the measured droplet velocity. This gives 8.83×10^{-7} kg m/s for $D_{0.5} \sim 500\,\mu$m and $V_{1\mathrm{m}} \sim 13.5$ m/s, which are deduced from Figure 3. Both diameter and velocity are measured in the absence of fire at a distance of 1 m from nozzle. The total momentum of the spray can be obtained by summing the individual droplet momentum values. This momentum value of the droplets was sufficient enough to reach the fuel surface.

Figure 6 shows the time series snapshots of the fire suppression conducted with nozzle 30200 injecting at a constant flow rate of 28 gpm *with* the calorimeter. Again, the image taken at $t = -0.33$ s shows the typical fire structure prior to the spray injection, and the image taken at

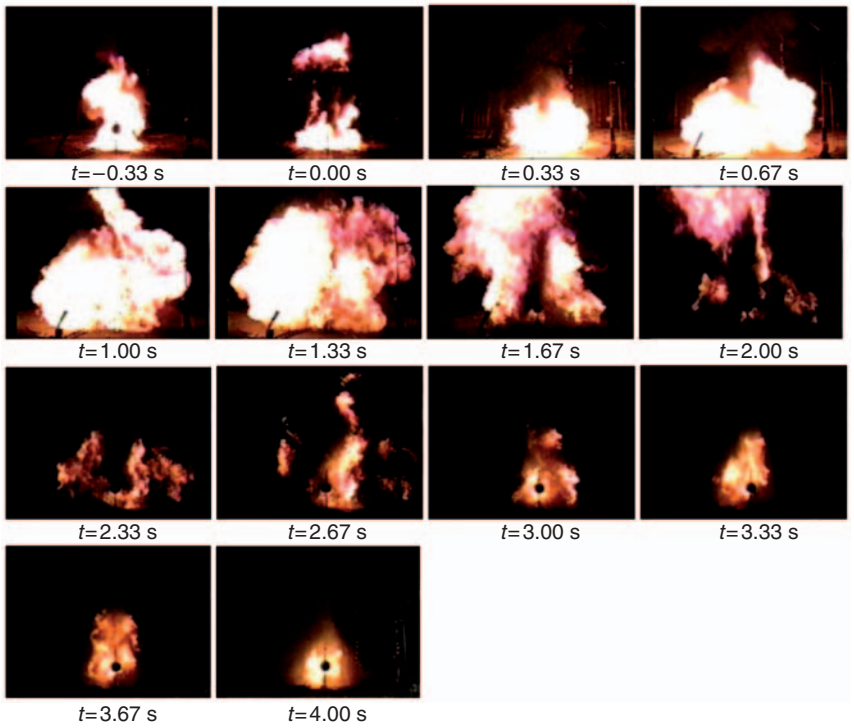

Figure 6. 90° spray injection at 100 psi with the calorimeter (Test 5). (Suppression is never achieved).

$t = 0.00$ s shows the fire structure when the water spray was first injected. In this case, the fire is not fully suppressed even though the nozzle's operating condition is the same as that in the previous case of Figure 5. The presence of the calorimeter makes it more difficult to suppress the fire. Notice again that when the spray reached the flame during $0.33\text{ s} \leq t \leq 1.67$ s in Figure 6, the fire intensity increased. Judging from the images in Figures 5 and 6, the enhanced fire intensity is comparable in both cases, except in the region below the calorimeter where we presume fuel-air mixing was enhanced due to the increase in flow turbulence produced by vortices underneath the calorimeter itself [16].

Figure 7 shows the time series snapshot of the fire suppression conducted with nozzle 30200 and the calorimeter under the 34 gpm injection pressure of Test 6. In this case, the fire was fully suppressed even with the calorimeter present because of sufficient spray momentum and mass flow rate; the suppression time was recorded at $t_{\text{supp}} = 1.67 \pm 0.33$ s. Note that the increased momentum of the spray

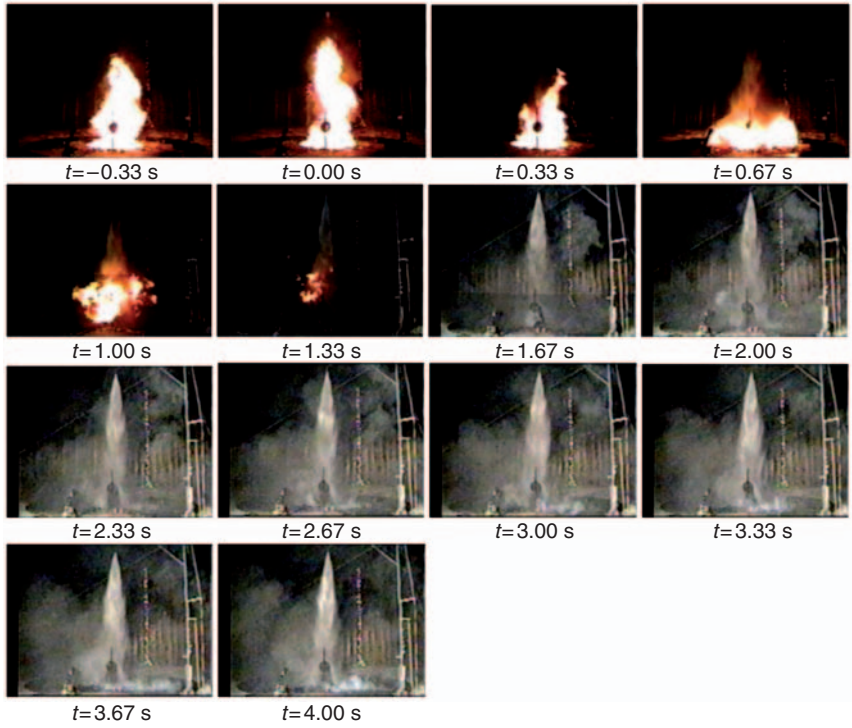

Figure 7. 90° spray injection at 155 psi with the calorimeter (Test 6). (Suppression is achieved around 1.67 s).

in Test 6, as compared to that of Test 5, did not appear to enhance the fuel-air mixing as substantially.

At the 34 gpm mass flow rate of Test 6, the mean droplet diameter and velocity 1 m downstream from the nozzle exit were estimated to be 400 μm and 14 m/s. A rough estimate of the individual droplet momentum gives 4.69×10^{-7} kg m/s. This momentum value is actually smaller than the one estimated for nozzle 30200 at 100 psi of Test 5, which was 8.83×10^{-7} kg m/s. Although the velocity of the droplet is slightly higher for Test 6 than for Test 5, the individual droplet momentum is more sensitive to droplet size (notice that the momentum is proportional to $D_{0.5}^3 V_{1m}$). As a result, the individual momentum of a droplet for Test 6 is smaller than that for Test 5. It should be, however, realized that the number of droplets increased because of the mass flow rate increase; therefore, the total momentum of the spray increased.

Based on the results for 28 gpm of Test 5 and 34 gpm of Test 6, it is inferred that increasing the total momentum of the spray, but decreasing an individual droplet momentum by high operating pressure actually reduces the intensity of the fire during suppresion. It may also be inferred that increasing the flow rate decreases the time to suppression, thus, increasing the efficiency of fire suppression. However, as it will be shownlater, it should be cautioned that the trend might not persist in some cases.

Figure 8 shows the time series snapshot of the fire suppression conducted *with* nozzle 30200 injecting at 39 gpm *without* a calorimeter below. This case is referred to as Test 3, in which the operating pressure is increased to 190 psi. From previous results, it may be supposed that increasing the flow rate from 34 to 39 gpm would result in a more efficient suppression condition, but the snapshots from Figure 8 show otherwise. The flame intensity was enhanced slightly with an even higher spray momentum. Furthermore, suppression was achieved at about $\Delta t_{\text{supp}} = 2.67$ s; this suppression time is greater than that of the 34 gpm case of Test 6 ($\Delta t_{\text{supp}} = 1.67$ s even *with* the calorimeter) and comparable to that of the 28 gpm case of Test 5 *without* the calorimeter ($\Delta t_{\text{supp}} = 3.00$ s). This surprising result indicates that a high value of the total momentum of the water spray can temporarily enhance the fire prior to suppression. This behavior is attributed to the smaller droplets, whose penetration against the fire was not as efficient as it was in Test 6. This behavior shows that there is an optimum droplet size best suitable for a given fire suppression scenario.

Figure 9 shows the time series snapshots of the fire suppression conducted with nozzle 30200 injecting at 39 gpm *with* a calorimeter below. In this case suppression was achieved at a slightly later time,

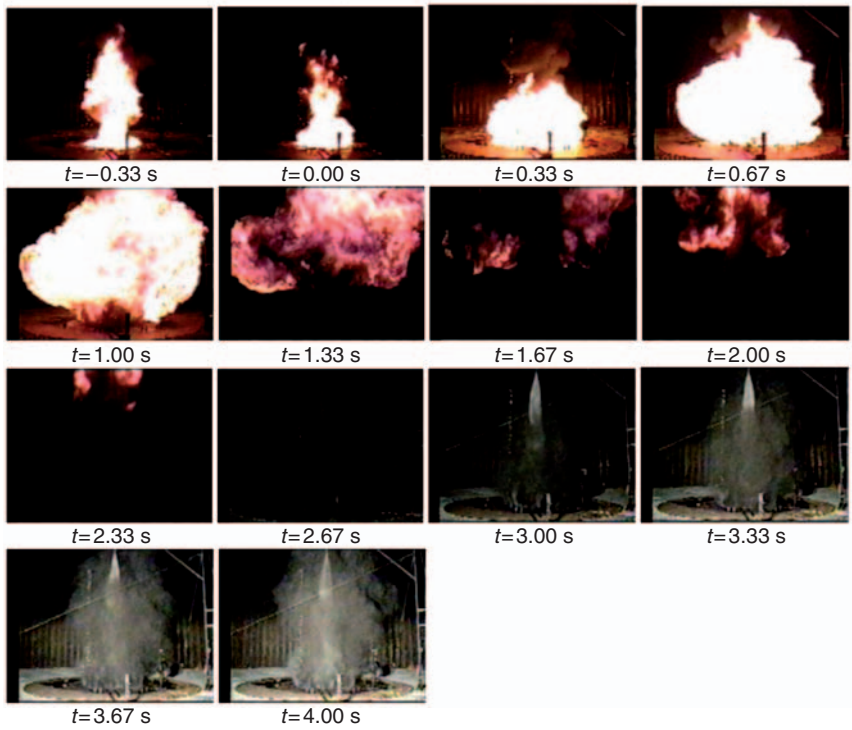

Figure 8. 90° spray injection at 190 psi without the calorimeter (Test 3). (Suppression is achieved approximately at $t = 2.7 \pm 0.33$ s).

$\Delta t_{\text{supp}} = 3.00$ s, than that *without* the calorimeter below. The flame intensity was also slightly more enhanced in this case because of the presence of an object. It is safe to conclude that the effect of the calorimeter at the high operating pressure of Test 3 is fairly insignificant.

Initially, it was thought that increasing the overall spray momentum at greater flow rate was absolutely desirable to achieve efficient suppression. However, Figures 7–9 indicate that the greater momentum of a spray is not always desirable because it may increase the intensity of the fire. Thus, increasing spray momentum is favorable only up to a certain limit condition, which we describe in terms of the optimum flow rate and droplet size. Any flow rate exceeding the optimum value would intensify the flame by agitating the fire.

Based on the aforementioned experiments, a rough critical line was constructed as shown in Figure 4. This critical line is defined as the point at which the suppression is achieved without the calorimeter.

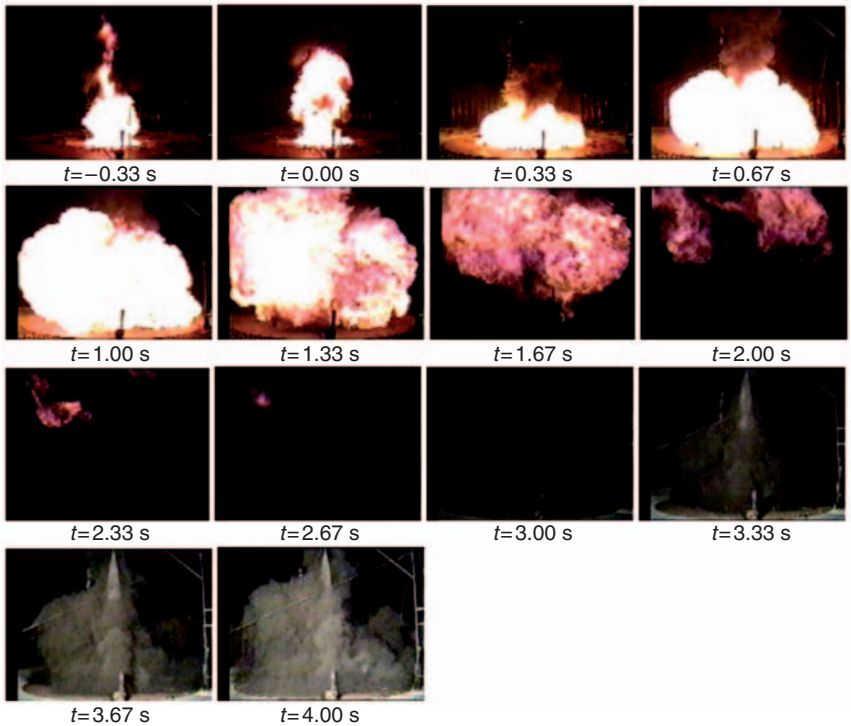

Figure 9. 90° spray injection at 190 psi with the calorimeter (Test 3). (Suppression is achieved approximately at $t = 3 \pm 1/3$ s).

In other words, the operating regime below the critical line would not yield suppression and the operating regime above the line would guarantee suppression for a case *without* the calorimeter. To guarantee suppression for a case *with* the calorimeter, a certain marginal tolerance – shifting to the upper right region with respect to the critical line in Figure 4 – needs to be considered. This tolerance should be estimated based on the experimental data.

Injection Angle of 45°

The suppression tests with a 45° injection angle were carried out to seek a nozzle configuration which may yield a better suppression performance; see Figure 2(a). The nozzle was set up such that the entire pool fire was covered under the spray impingement area. The height of the nozzle remained the same as that of the previous 90° configuration,

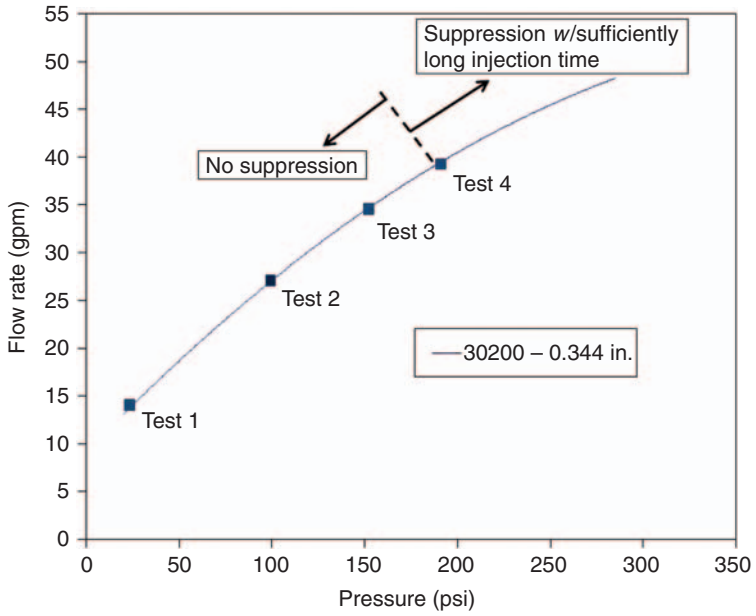

Figure 10. *Critical line for suppression for 45° spray injection.*

and, thus, the spray travel distance to the calorimeter and the pool fire was increased by a factor of $\sqrt{2}$; this distance may be far enough to adversely affect the suppression condition. The operating pressure was set to 25 psi and increased up to 190 psi with the nozzle diameter of 0.344 in.

Figure 10 summarizes the test results conducted with the 45° spray angle. The fire was suppressed at 155 psi only *without* the calorimeter, but these results were not repeatable. Suppression was consistently achieved when the operating pressure was >190 psi only for the case *without* the calorimeter. In this case the suppression time reached nearly 10 times the suppression time of the case with 90° injection angle, based on the comparison of the results from Test 3 of Table 2 (90° injection) and Test 4 of Table 3 (45° injection). Due to limitation in suppression system, higher operating pressures were not possible with nozzle 30200. It is uncertain how high the operating pressure should be to suppress the fire consistently with the calorimeter in place at this given 45° configuration.

Figures 11 and 12 show the time series snapshot of the fire suppression conducted with nozzle 30200 at 45° injecting at 39 gpm

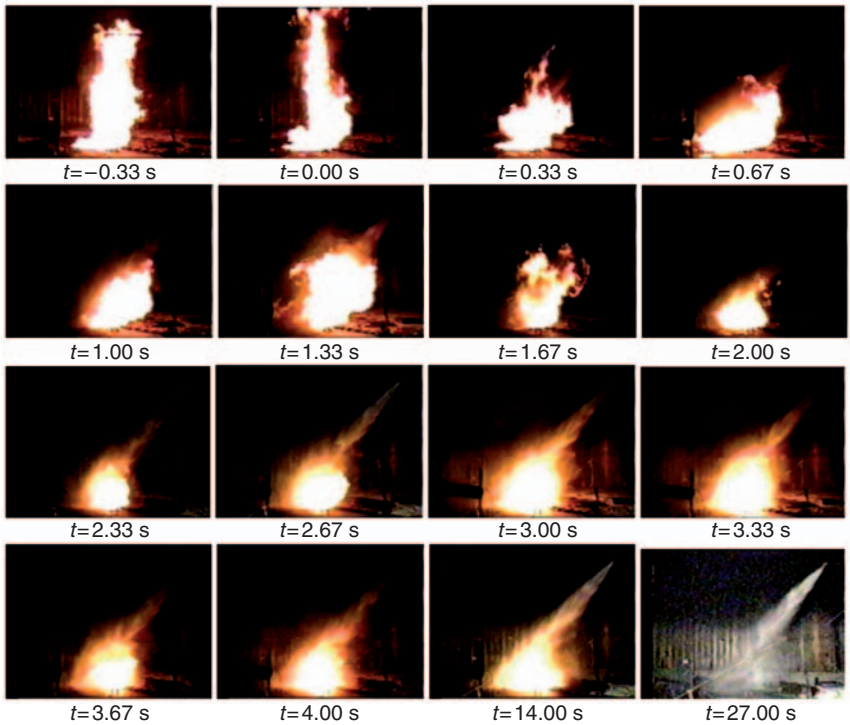

Figure 11. 45° Spray Injection at 190 psi without the Calorimeter (Test 4). (Suppression is achieved at t = 27 ± 1/3 s).

with and without a calorimeter below, respectively. Notice that in both figures, the initial intensification that was observed in the 90° angle tests is not present, indicating insufficient spray momentum. Also, the region of the fire's influence appears to be much smaller than results of the 90° configuration suggest, and a constant size fire below the calorimeter is present for a relatively long period of time.

The reason for the poor performance of the 45° nozzle configuration is attributed to several factors. First, the spray travel distance was comparatively long with the 45° nozzle. With such a long distance, the spray momentum can be lost, especially when the spray droplets are confronted against a vibrantly rising buoyant flame. Second, the spray was unevenly distributed across the fire, which means that the spray may have helped stir the fire more vigorously, enhancing the mixing and burning rates. As a result, the fire became difficult to suppress.

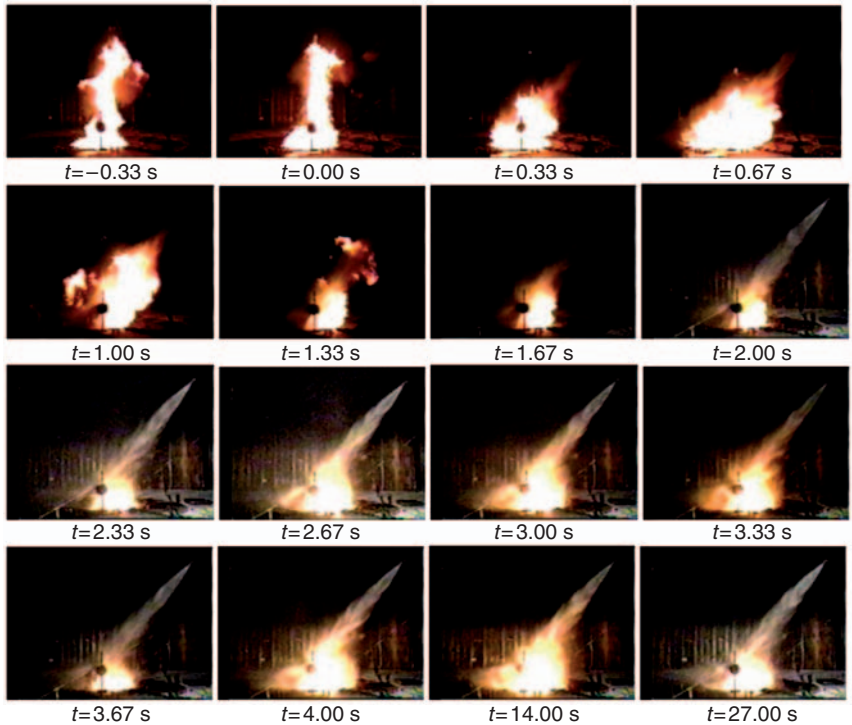

Figure 12. 45° spray injection at 190 psi with the calorimeter (Test 4). (Suppression is never achieved).

SIMULTATION RESULTS

Two Phase Flow Fire Suppression Modeling

Numerical simulations are conducted using Sandia's fire field modeling code, VULCAN (*ComputIT*, Co., Trondheim, Norway). The Eulerian gas phase is solved assuming the Temporally Filtered Navier-Stokes (TFNS) turbulence closure model [17]. The 'Eddy Dissipation Concept' (EDC) combustion model of Ertesvag and Magnussen [18] is used to model turbulent combustion. Soot formation and absorption properties are based on the work of Tesner [19], and a discrete transfer method is used to solve for the radiation heat transfer.

Liquid fuel vaporization rates were computed using the model described in Brown and Vembe [20], which predicts pool evaporation on the basis of convective and radiative flux at the pool surface. This model has been found to reasonably approximate the vaporization

behavior of liquid fuels to incident flux. However, the model will not correctly simulate the effects of impinging liquid water on the fuel surface. The model was tuned to produce realistic and accurate mass fluxes or fuel release rate at steady state by adjusting the radiation absorption coefficient, on the basis of the experimental values. Although examples of evaporation models exist in the literature, accurate pool vaporization models have yet to be fully validated for this class of fire.

The model of discrete transfer method of Shah and Lockwood is used to solve the radiative transport equation, and gas and soot properties are extracted from open literature models [21,22]. Soot is computed because it contributes to the radiation [22]. The Lagrangian model radiation interactions are not modeled in the version of the code used in this study, so the droplet thermal interactions with the flame are purely convective.

The gas-phase flow is calculated on an Eulerian staggered Cartesian grid using the pressure correction method of the SIMPLE algorithm [23]. Upwinding and centered schemes that approach second-order spatial accuracy are used for the convective and diffusion terms, respectively, for solving the transport differential equations.

The water spray model is based on a Lagrangian stochastic separated flow approach [24,25]. The concept of a 'group parcel' representing collection of droplets of similar sizes is adopted to reduce computational cost. The motion of parcels is advanced under the influence of modeled turbulent fluctuations in the gas-phase properties. Maxey and Riley's [26] momentum equation for a small rigid sphere in a non-uniform flow is used. Evaporation is modeled using a thin skin model with standard convective correlations of heat and mass transfer. Droplet–droplet collisions are modeled using the model of Brazier-Smith et al. [27]. This approach only accounts for either droplet–droplet 'bouncing' or 'coalescence,' and not the droplet–droplet 'shattering' effect, which produces additional drops. The 'shattering' effect may become important for head-to-head colliding sprays, but can be neglected in this case [28]. Droplet-wall impacts are also modeled, based on refs. [29–31]. Since all droplets are typically moving in the same direction in our 'dilute' spray, shattering is unlikely to occur. Droplet breakup due to aerodynamic forces is modeled using the Taylor Analogy Breakup (TAB) Model of O'Rourke and Amsden [32].

Particle turbulence interaction models are introduced at the parcel and sub-parcel level to account for the effect of local fluctuations in the velocity field, while the rest of the thermo-physical variables are approximated by their corresponding time averaged values. The velocity-fluctuation models serve to increase the droplet dispersion, mimicking

the effects of unresolved turbulent eddies. These unresolved turbulent motions are significant for the present high-pressure sprays that generate substantial turbulent kinetic energy. The unresolved turbulent motions are decomposed into parcel and sub-parcel models. The parcel turbulence model accounts for the effects of turbulent eddies perturbing the parcel trajectory and is based on the random walk model of Gosman and Ioannides [33], as modified by Shuen et al. [34]. Within a parcel, a Gaussian spatial distribution of particles is assumed. The standard deviation of this spatial distribution evolves with time for each parcel as discussed by Zhou and Yao [35].

The VULCAN suppression model is based on the concept of a critical Damkohler number, where the Damkohler number represents the ratio between the chemical and fluid mixing time scales [36]. This suppression model captures the physics of both oxygen depletion and flame cooling in fire suppression because both act to increase the chemical time scales. The chemical time scales were determined by conducting a series of computations of the blowout limits for a perfectly stirred reactor (PSR) [37,38]. Further details on the suppression model are available in ref. [24].

Computational Details

The water spray was injected directly above the fire centered at $x_{inj} = y_{inj} = 0$, and $z_{inj} = 5.0$ m, and the droplet velocity was varied from $U_{inj} = 20$ m/s to 60 m/s. The time step used in the gas-phase simulation was allowed to vary between 0.01 s and 0.0001 s to maintain a peak Courant number of 0.5 and below. The sub-cycling time step for the liquid phase was approximately $\Delta t_{\text{liq}} \approx \Delta t_{\text{gas}}/100$ s, set by the stability criterion implemented in the fire suppression code at the given maximum injection speed. The grid was stretched to provide fine resolution near the pool fire, for a computational node count of 168, 116 (or $53 \times 52 \times 61$). The cone angle of the spray was set at $\theta = 30^{\text{o}}$, and the spray injection was initiated at $t = 5$ s. A total of 50,000 computational parcels were injected during 5 s of spray injection (or 10,000 parcels/s). The total number of water droplets ranged from 13.0×10^6 to 1.1×10^9, which yielded an average value of 2×10^2 to 21×10^3 droplets per parcel. The distribution of initial droplet sizes was assumed to be of the Rosin–Rammler distribution shape (i.e., $\text{PDF}(D) = (qD^{q-1}/X^q)\exp(-(D/X)^q)$, where D is the droplet diameter and X is the characteristic or mean droplet size with the corresponding dispersion coefficient of $q = 1.8$, deduced from the experimental data obtained for a typical commercial nozzle of the *Spray System* Co., IL.

A few of the experimental cases were selected for simulation. The cases with the calorimeter were avoided because the deposition, heat transfer, and spread of liquid on the calorimeter introduced additional challenges to the problem that could not be well described by the present model. To limit the scope, the 90° spray cases were selected for our computational analysis.

JP8 Pool Fire Predictions

Simulated results shown in Figure 13 indicate the quasi-steady state temperature of burning gas at various physical heights, $z = 0.141$, 0.840, and 2.085 m. Note that no water spray was injected for this particular simulation. It seems that the quasi-steady state was reached at about $t = 5$ s and, thus, spray injection is initiated at this instant, which corresponds to $t = 0$ s of the experimental time in Figures 5–8. Locations selected are in a regime of increasing predicted temperature with height.

Test 3: High Injection Pressure

In the simulation, nozzle model no. 30200 (*Spray System*, Co., IL), with a nozzle diameter $d = 0.344$ in., was modeled. The operating condition

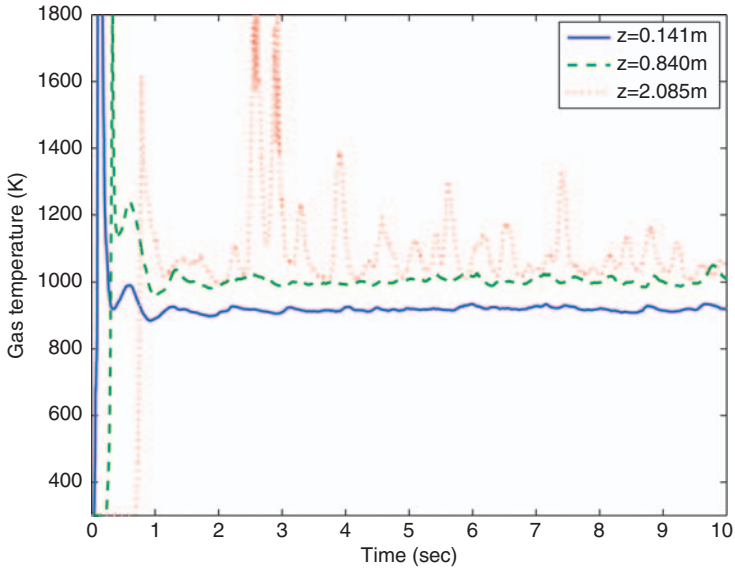

Figure 13. Time histories of the local gas temperature at the pool fire center, $x = y = 0$ plane for various heights. A quasi-steady state is reached at about $t = 5$ s.

consisted of the following: operating pressure was 190 psi, mass flow rate was 2.46 kg/s, the mean diameter and the dispersion coefficient of the Rosin–Rammler distribution were 370 μm and 1.8, respectively. Due to the relatively high-injection pressure of the nozzle, the initial droplet size at the nozzle exit was relatively small and the droplet had a high evaporation rate, which induced rapid cooling of both the flame and pool surface.

Figure 14 shows gas temperature spikes observed subsequent to the initiation of the water spray at $t = 5$ s – see the results during $5.5\text{ s} < t < 6.0\text{ s}$ for $z = 0.141$ and 0.840 m, which are relatively low in height. Because the water spray nozzle is located at $z = 5.0$ m, the gas in the proximity of the nozzle is cooled by the water spray first, while the lower parts of the flame undergo enhanced combustion, which is presumably due to the ample supply of air from top to bottom and increased spray momentum, which contributes to the enhanced turbulent fuel-air mixing. This explanation of enhanced turbulence for Figure 14 is consistent with the qualitative volume-rendered temperature results of the simulations shown in Figure 15.

As expected, upon spray injection at $t = 5$ s, the flame shape changed due to the spray momentum projection toward the flame.

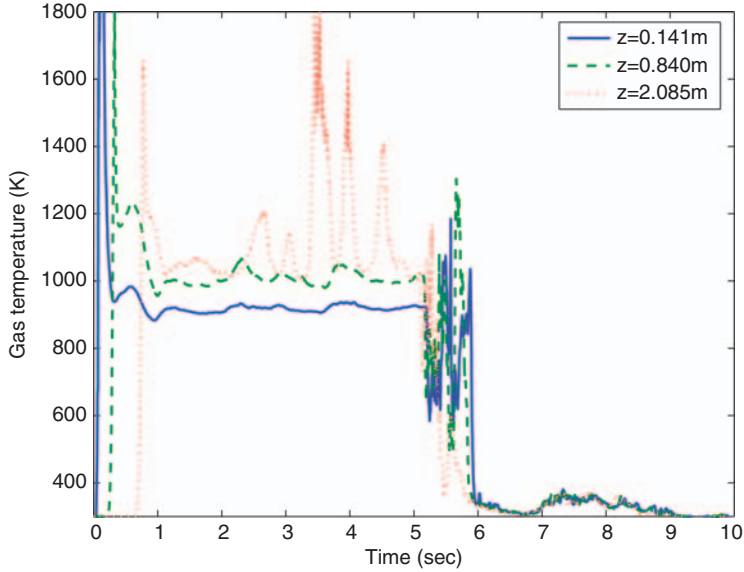

Figure 14. Time histories of gas temperature at the pool fire center for various heights for Test 3. Gas temperature experiences a sudden decrease when subject to water spray.

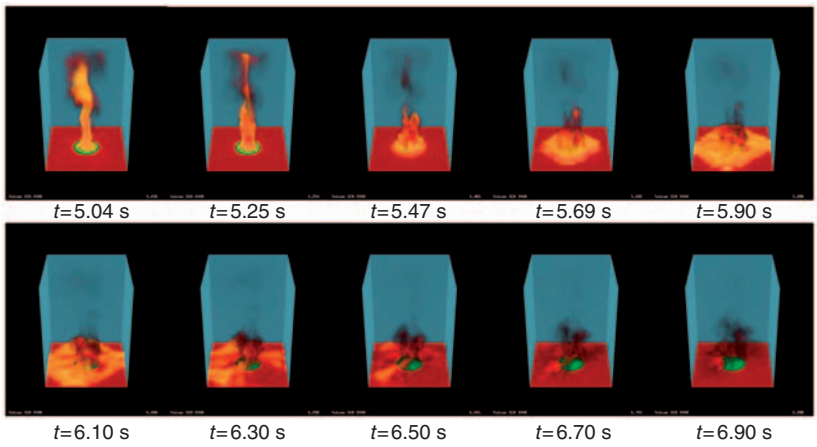

Figure 15. Simulation result for Test 3. Suppression was achieved at $\sim t = 7\,s$*, yielding the suppression time of* $\Delta t_{supp} = 2\,s$.

The spray momentum was large enough to overcome the rising buoyancy force of the flame. As a result, within a fraction of a second after the injection (i.e., $t = 5.9\,s$), the flame column quickly disappeared and flattened near the pool surface. At about $t = 7\,s$, fire was nearly suppressed with a small flame still surviving at the pool's edge, which caused an increase in the gas temperature at $t = 7\,s$, as manifested in Figure 14. The fire was eventually extinguished, finally reaching 300 K gas temperature at all locations.

Flame enhancement due to spray injection was also observed in the experiment, as shown in Figure 8. The 'fireball,' or intensification, was at its maximum size 1 s after the water spray injection ($t = 1\,s$ in the experimental time corresponding to $t = 6\,s$ in simulation time in Figure 15). Based on the snapshots from Figure 8, the flame seems to be completely suppressed at the pool surface at $t > 1.33\,s$ (though it is possible a few small flames still may have remained at the pool). For $t > 1.33\,s$, only the remaining fireball continued to rise, and eventually dissipated. Currently, we do not have the quantitative experimental data of local gas temperatures and, thus, cannot make a direct comparison between the model and experimental results. However, under the given injection pressure of 190 psi in Test 3, the model predicted the extinguishment of fire, which was the case in the actual experiment. In addition, the model predicted the suppression time of $\Delta t_{supp} = 2\,s$, which is in fairly good agreement with the experimental suppression time of $\Delta t_{supp} = 2.67\,s$ from Table 4. Nevertheless, flame enhancement due to spray injection is not observed in the simulation results.

Table 4. Comparison of suppression time, Δt_{supp}, from experiments and simulations for the 90° nozzle configuration.

Test no.	With calorimeter (experiment)	Without calorimeter (experiment)	Without calorimeter (simulation)
1	No suppression	No suppression	N.A.
2	4.00 s	N.A.	N.A.
3	3.00 s	2.67 s	2.00 s
4	No suppression	No suppression	No suppression
5	No suppression	3.00 s	5.00 s
6	1.67 s	N.A.	N.A.
7	No suppression	No suppression	N.A.

Test 4: Low Injection Pressure

Test 4 was simulated for the following initial conditions. The nozzle model was no. 30200 (*Spray System*, Co., IL), nozzle diameter was $d = 0.344$ in., injection pressure was 25 psi, mass flow rate was 0.883 kg/s, the volume average mean diameter of droplets was $D_{0.5} = 870\ \mu$m, and the dispersion coefficient of the Rosin–Rammler distribution was $q = 1.8$. Due to the relatively low injection pressure of the nozzle, the initial droplet size at the nozzle exit was relatively large. Thus, we expected less efficient suppression, as opposed to the excellent suppression result of the previous Test 3.

Figure 16 shows the temporal changes of the gas temperature for Test 4 at various heights. The mass flow rate is substantially reduced to 14 gpm, as compared to the 39 gpm from Test 3, because of the low injection pressure. Thus, we expected a dramatic reduction in the spray momentum and lower quantities of water evaporating in the fire. Suppression was not achieved, although the flame indeed recognized the presence of the water spray, as suggested by the fluctuation in the flame temperature of the baseline fire case. The flame's buoyancy force was strong enough or spray momentum was too weak to significantly change the morphology of the flame, a fact suggested by visualizations in Figure 17. This nonsuppression of the fire was predicted by our simulation, consistent with the experimental result of Test 4 (Table 4).

Test 5: Intermediate Injection Pressure

Two extreme cases (i.e., high 190 psi of Test 3 and low 25 psi of Test 4) have led further to investigate numerically the effect of moderate injection pressure on suppression. An intermediate injection pressure

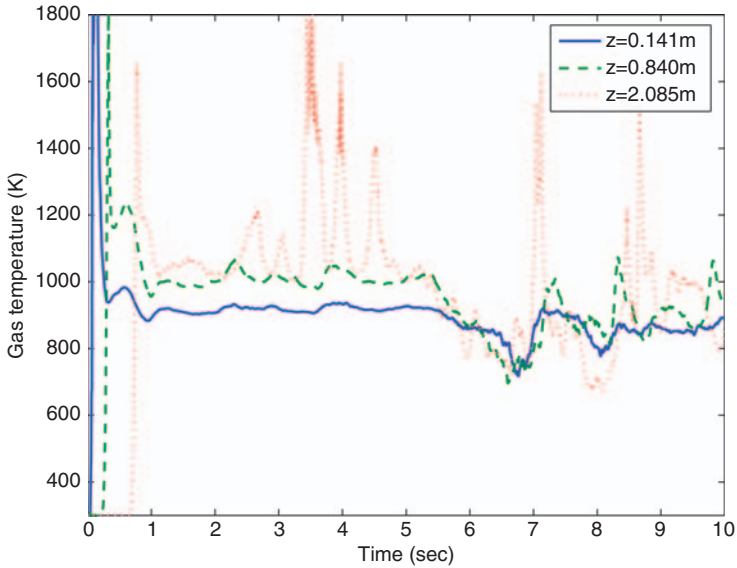

Figure 16. Time histories of gas temperature at the pool fire center for Test 4.

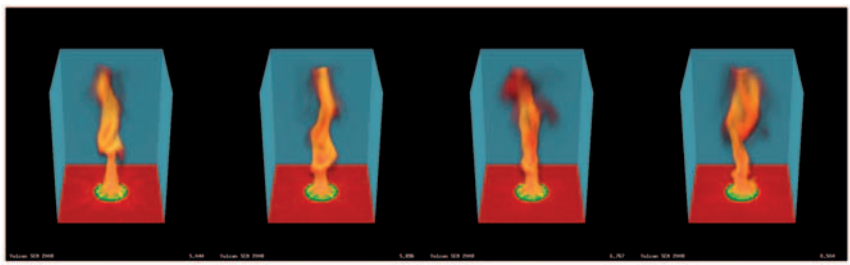

Figure 17. Simulation result for Test 4. Suppression was not achieved during the time of injection at $t = 5$ s to the end of the simulation at $t = 10$ s.

(i.e., 100 psi of Test 5) was considered and applied to a fire suppression scenario. Simulation of Test 5 employed nozzle model no. 30200 ($d = 0.344$ in.) operating at a pressure of 100 psi and a mass flow rate of 1.77 kg/s, with an average VMD of $D_{0.5} = 490\,\mu$m, and a dispersion coefficient of the Rosin–Rammler distribution $q = 1.8$. Due to the intermediate injection pressure, we expected a longer suppression time than that of Test 3, if ever suppression was achieved or, at least, a clear change in flame morphology.

Figure 18 shows the qualitative computational results of Test 5. The fire appears to survive until $t = 7.9$ s, and suppression appears

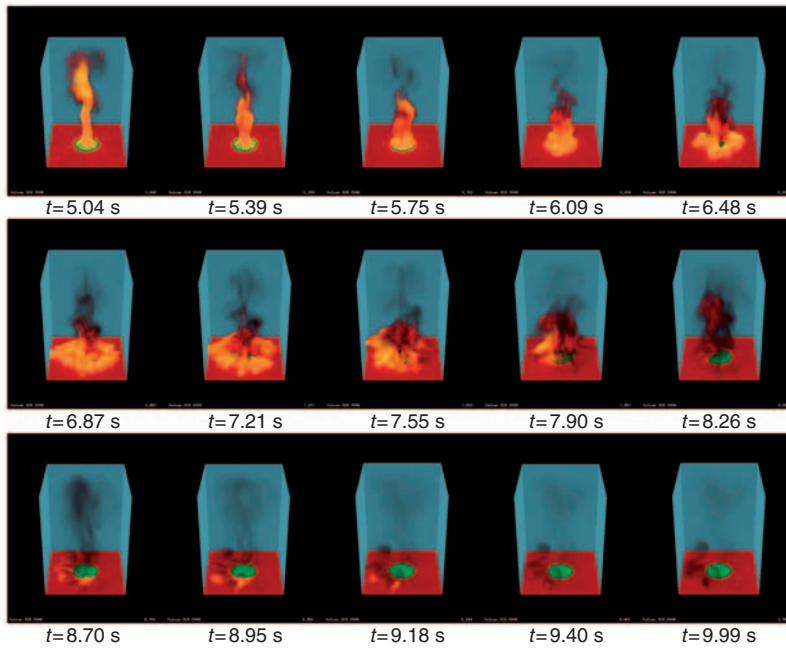

Figure 18. Simulation result for Test 5 (Nozzle no. 30200, d = 0.344 in., 100 psi, 1.77 kg/s, X = 490 μm, and q = 1.8). The fire was suppressed at about t = 9.40 s. Relatively lower injection pressure (as compared to Test no. 3) yielded a delay in suppression time.

complete at $t = 8.26$ s. A small flame at the pool's edge 're-ignited' the pool, whose effect is shown in the snapshots at 8.70–9.18 s. The fire appears completely suppressed at $t = 9.4$ s. Excluding the temporal rise in gas temperature due to the re-ignition, suppression was said to be achieved at about $t = 8.0$ s, which was a longer duration than that recorded in Test 3. This result was expected because of the lower injection pressure of Test 5. This longer suppression duration of the model result was consistent with what was experimentally observed for Test 5, as indicated in Table 4; the intermediate operating pressure resulted in longer suppression time than that of the high pressure case Test 3. Again, no subsequent intensification is observed to rise from near the pool surface as observed in the experiments.

Modeling Summary

We suspect that several unique features of our code lead to the positive agreement of the model result to the experiment results.

A fuel vaporization model that responds to the energy input is thought to be critical in this type of modeling. It inhibits the fuel from vaporizing when the feedback from the fire diminishes. Broadly applicable models to this extent have yet to be demonstrated. Improvements in modeling the response of fuels are critical to the predictability of such scenarios.

Physical elements missing from the present model may yet prove to be significant. We believe that the particle/radiation interaction could be significant since the water droplet fraction may be high in the fire region. The interactions between the spray and the liquid pool may also be important, as suggested in a previous work [5]. Higher resolution modeling may also be important for fully capturing the gas-phase dynamics.

The good comparison found between the model and experiment as suggested by Table 4 suggests that it is possible to achieve a reasonable reproduction of the bulk characteristics of spray suppression with the current suite of 3D modeling tools. The complexity of the interaction among the various physical aspects of the model inhibits this study from quantifying the relative importance of the various mechanisms involved in the suppression of the fire. Indeed, it may be difficult to widely validate a suppression model without considering various parameters, such as fuel types, configurations, and scales, upon which suppression mechanisms are highly dependent. Because detailed measurements are often unavailable, integral metrics may be found to be most useful. Fire prediction and fire suppression involve very complex multi-phase interrelated physics and chemistry, which interact across wide ranges of length and time scales. As modeling becomes more mature with increasingly accurate physical models and quantified validations, it may be used more frequently in the design and study of fire suppression and protection systems.

CONCLUSIONS

A series of water spray fire suppression benchmark experiments were performed. Boundary and temporal data were measured to support the development and validation of the flame model used for the evaluation of the Sandia's fire suppression code, VULCAN. A total of 12 fire suppression cases were tested. Test parameters included the nozzle size, nozzle orientation, operating pressure, and the presence or absence of a cylindrical calorimeter inside the fire. Results obtained from the application of a 90° and a 45° spray angle were significantly different. Results from the 90° spray angle configuration showed suppression above a critical line, expressed as a function of pressure and suppressant

flow rate. Operating in the regime below the critical line did not yield complete suppression, and operation in any regime above the line guaranteed suppression for the case *without* the calorimeter. To guarantee suppression for the case *with* the calorimeter, a higher mass flow rate needs to be considered. Except in the region near the critical line, the presence of the calorimeter did not seem to have a great effect on suppression. In the region below the critical line, no suppression is achieved, regardless of the presence of an object. Similarly, suppression was achieved regardless of the presence of the calorimeter in the region above the critical line. As for the 45° configuration results, suppression was much more difficult to achieve because of the droplets' longer travel distance and their asymmetric dispersion, which caused unwanted vortices behind the calorimeter. A general conclusion can be drawn that high nozzle pressure or high mass flow rate of water alone cannot guarantee suppression. In other words, suppression is guaranteed only if reasonably high values of *both* injection pressure and mass flow rate (or sufficiently large nozzle diameter) are secured. The suppression model produced suppression time results that were consistent with the experiments for high, low, and intermediate injection pressures, which correspond to experimental Tests 3, 4, and 5, respectively.

ACKNOWLEDGMENTS

This study was sponsored in part by the Department of Defense (DTRA) and was performed at Sandia National Laboratories. Sandia is a multiprogram laboratory operated by Sandia Corporation, a Lockheed Martin Company, for the United States Department of Energy under Contract No. DE-AC04-94AL85000. Sam Yoon acknowledges that part of this research was supported by Basic Science Research Program through the National Research Foundation of Korea (NRF) funded by the Ministry of Education, Science and Technology (2009-0063169) and KRF 2008-313-D00135.

REFERENCES

1. Montreal Protocol on Substances that Deplete the Ozone Layer. Final Act, Montreal, Canada, United Nations Environmental Program (UNEP), September 1987. Available at: http://ozone.unep.org/pdfs/Montreal-Protocol2000.pdf
2. Grant, G., Brenton, J. and Drysdale, D. (2000). Fire Suppression by Water Sprays, *Progress in Energy and Combustion Science*, **26**: 79–130.

3. Yoon, S.J., Kim, H.Y., DesJardin, P.E., Hewson, J.C., Tieszen, S.R. and Blanchat, T.K. (2007). Unsteady RANS Modeling of Water-spray Suppression for Large-scale Compartment Pool Fires, *Atomization and Sprays*, **17**(1): 1–45.
4. Rasbash, D.J., Rogowski, Z.W. and Stark, G.W.V. (1960). Mechanisms of Extinction of Liquid Fires with Water Sprays, *Combustion and Flame*, **4**: 223–234.
5. Novozhilov, V., Harvie, D.J.E., Green, A.R. and Kent, J.H. (1997). A Computational Fluid Dynamic Model of Fire Burning Rate and Extinction by Water Sprinkler, *Combustion Science and Technology*, **123**: 227–245.
6. Prasad, K., Li, C. and Kailasanath, K. (1999). Simulation of Water Mist Suppression of Small Scale Methanol Liquid Pool Fires, *Fire Safety Journal*, **33**: 185–212.
7. Ndubizu, C.C., Ananth, R. and Tatem, P.A. (2000). The Effects of Droplet Size and Injection Orientation on Water Mist Suppression of Low and High Boiling Point Liquid Pool Fires, *Combustion Science and Technology*, **157**: 63–86.
8. Back, G.G., Beyler, C.L. and Hansen, R. (2000). A Quasi-steady-state Model for Predicting Fire Suppression in Spaces Protected by Water Mist Systems, *Fire Safety Journal*, **35**: 327–362.
9. Back, G.G. and Hansen, R. (2000). The Capabilities and Limitations of Total Flooding, Water Mist Fire Suppression Systems in Machinery Space Applications, *Fire Technology*, **36**: 8–23.
10. Heskestad, G. (2003). Extinction of Gas and Liquid Pool Fires with Water Sprays, *Fire Safety Journal*, **38**: 301–317.
11. Adiga, K.C., Hatcher, R.F., Sheinson, R.S., Williams, F.W. and Ayers, S. (2007). A Computational and Experimental Study of Ultra Fine Water Mist as a Total Flooding Agent, *Fire Safety Journal*, **42**: 150–160.
12. Ricks, A.J. and Blanchat, T.K. (2007). Hydrocarbon Characterization Experiments in Fully Turbulent Fires, SANDIA Report, SAND2007-2391, Albuquerque, New Mexico.
13. DiNenno, P.J., Drysdale, D., Beyler, C.L., Walton, W.D., Custer, R.L.P., Hall, J.R. and Watts, J.M. (2002). The SFPE Handbook of Fire Protection Engineering, Society of Fire Protection Engineers, NFPA No. HFPE-02, ISBN: 087765-451-4.
14. Blinov, V.I. and Khudiakov, G.N. (1961). Diffusion Burning of Liquids, U.S. Army Translation, NTIS No. AD296762.
15. Hottel, H.C. (1959). Certain Laws Governing Diffusive Burning of Liquids, *Fire Research Abstracts and Reviews*, **1**: 41.
16. Tieszen, S.R., Nicolette, V.F., Gritzo, L.A., Holen, J.K., Murray, D. and Moya, J.L. (1996). *Vortical Structures in Pool Fires: Observation, Speculation and Simulation*, SAND96-2607.
17. Tieszen, S.R., Domino, S.P. and Black, A.R. (2005) Validation of a Simple Turbulence Model Suitable for Closure of Temporally-filtered Navier-stokes Equations Using a Helium Plume, SAND2005-3210.
18. Ertesvag, S. and Magnussen, B.F. (2000). The Eddy Dissipation Turbulence Energy Cascade Model, *Combustion Science and Technology*, **159**: 213–235.

19. Tesner, P.A. (1994). Growth Rate of Soot Particles, *Combustion Science and Technology*, **97**: 243–245.
20. Brown, A.L. and Vembe, B.E. (2006). Evaluation of a Model for the Evaporation of Fuel from a Liquid Pool in a CFD Fire Code, In: *Proceedings of the ASME International Mechanical Engineering Congress & Exposition*, Chicago, IL, USA, IMECE2006-15147.
21. Leckner, B. (1972). Spectral and Total Emissivity of Water Vapor and Carbon Dioxide, *Combustion and Flame*, **19**: 33–48.
22. Magnussen, B.F. and Hjertager, B.H. (1977). On Mathematical Modeling of Turbulent Combustion with Special Emphasis on Soot Formation and Combustion, In: *16th Symposium (International) on Combustion*, The Combustion Institute, MIT, Cambridge, MA, 15–20 August, pp. 719–729.
23. Patankar, S.V. (1980). *Numerical Heat Transfer and Fluid Flow*, Taylor & Francis, New York.
24. DesJardin, P.E. and Gritzo, L.A. (2002). A Dilute Spray Model for Fire Simulations: Formulation, Usage and Benchmark Problems, Technical Report, Sandia National Laboratories, Albuquerque, SAND2002-3419.
25. Yoon, S.S., Hewson, J.C., DesJardin, P.E., Glaze, D.J., Black, A.R. and Skaggs, R.R. (2004). Numerical Modeling and Experimental Measurements of a High Speed Solid-cone Water Spray for Use in Fire Suppression Applications, *International Journal of Multiphase Flow*, **30**: 1369–1388.
26. Maxey, M.R. and Riley, J.J. (1983). Equation of Motion for a Small Rigid Sphere in a Non-uniform Flow, *Physics of Fluids*, **26**: 883–889.
27. Brazier-Smith, P.R., Jennings, S.G. and Latham, J. (1972). The Interaction of Falling Water Drops: Coalescence, *Proceedings of the Royal Society A*, **326**: 393–408.
28. Georjon, T.L. and Reitz, R.D. (1999). A Drop-shattering Collision Model for Multidimensional Spray Computations, *Atomization and Sprays*, **9**: 231–254.
29. Yoon, S.S., DesJardin, P.E., Presser, C., Hewson, J.C. and Avedisian, C.T. (2006). Numerical Modeling and Experimental Measurements of Water Spray Impact and Transport over a Cylinder, *International Journal of Multiphase Flow*, **32**: 132–157.
30. Yoon, S.S., Jepsen, R.A., Nissen, M.R. and O'Hern, T.J. (2007). Experimental Investigation on Splashing and Nonlinear Fingerlike Instability of Large Water Drops, *Journal of Fluids and Structures*, **23**: 101–115.
31. Brown, A.L., Jepsen, R.A. and Yoon, S.S. (2008). Modeling Large-scale Drop Impact: Splash Criteria and Droplet Distribution, ILASS Americas, In: *21st Annual Conference on Liquid Atomization and Spray Systems*, May, Orlando, Florida, USA.
32. O'Rourke, P.J. and Amsden, A.A. (1987). The TAB Method for Numerical Calculation of Spray Droplet Breakup, SAE Technical Paper, 872089.
33. Gosman, A.D. and Ioannides, E. (1981). Aspects of Computer Simulation Of Liquid-fueled Combustion, In: *19th AIAA Aerospace Science Meeting*, St. Louis, MO, AIAA-81-0323.
34. Shuen, J.S., Chen, L.D. and Faeth, G.M. (1983). Evaluation of a Stochastic Model of Particle Dispersion in a Turbulent Round Jet, *AIChE Journal*, **29**: 167–170.

35. Zhou, A. and Yao, S.C. (1992). Group Modeling of Impacting Spray Dynamics, *International Journal of Heat Mass Transfer,* **35**: 121–129.
36. Koutmos, P. (1999). Simulations of Turbulent Methane Diffusion Flames with Local Extinction Effects, *Fluid Dynamics Research*, **24**: 103–119.
37. Kee, R.J., Rupley, F.M. and Miller, J.D. (1989). CHEMKIN II: A Fortran Chemical Kinetics Package for the Analysis of Gas-phase Chemical Kinetics, Technical Report SAND89-8009, Sandia National Laboratory, Livermore, CA.
38. Glaborg, P., Kee, R.J., Grcar, J.F. and Miller, J. (1986). PSR: A Fortran Program for Modeling Well Stirred Reactors, Technical Report SAND85-8209, Sandia National Laboratory, Livermore, CA.

BIOGRAPHIES

Sam S. Yoon

Dr Sam Yoon is an associate professor in the School of Mechanical Engineering at Korea University, Seoul Korea. He obtained his undergraduate (BS) and graduate (MS and PhD) degrees from Colorado School of Mines and Purdue University, respectively. During his stay at Sandia National Lab from 2002 to 2005 as a post-doctoral fellow, he worked on fire suppression research. His current research interests include fire suppression modeling, spray coating, and fluidized bed reactor.

Victor Figueroa

Victor G. Figueroa obtained a B.S. in Mechanical Engineering from Turabo University (Puerto Rico) and an M.S. in Mechanical Engineering from the University of New Mexico. For the past 9 years he has been working in the Fire Science and Aerosol Department at Sandia National Laboratories, conducting both experiment and simulation work in the fire sciences and other related fields. His research interests include fire dynamics, inverse heat transfer, and quantification of experiment measurement uncertainty.

Alexander L. Brown

Dr Alexander Brown is a senior member of the technical staff in the Fire & Aerosol Science Department at Sandia National Laboratories. He obtained his BS, MS, and PhD degree in Mechanical Engineering at Brigham Young University, University of Utah, and University of Colorado at Boulder, respectively.

Thomas K. Blanchat

Dr Thomas Blanchat is a principle member of the technical staff in the Fire & Aerosol Science Department at Sandia National Laboratories. He obtained all his degrees (BS, MS, and PhD) from Texas A&M University. His main research interest is in experimental assessment of thermal hazard from hydrocarbon and LNG pool fires.